Cooperative topological accumulation of vacancies in honeycomb lattices

Ottorino Ori* [1,2], Franco Cataldo [1], Mihai V. Putz* [2,3], Forrest H. Kaatz [4], Adhemar Bultheel [5]

Abstract

Present topological study focuses on the formation mechanism of clusters of vacancies in graphenic layers. An original effect that explains both accumulation and *self-healing* of vacancies represents the original outcome of our investigation whose results, based on the long-range topological properties of the honeycomb lattices, are applicable to defective graphene sheets and general honeycomb lattices when other elements other than carbon are present. Some speculations about the role of long-range bondonic states in such a kind of lattices contribute to the understanding of electronic and transport properties in graphenic nanomaterials

Key words: Honeycomb Lattices, Nanographene, Vacancy Cluste rs, Topological Efficiency, Cooperative vacancies, graphene self-healing, Bondon

1 Introduction

Defects in graphite single-layer (graphene) represent an important investigation topic since 2008 when Zettl and coworkers introduced an innovative method for transmission electron mi-

[1] Actinium Chemical Research, Rome, Italy
[2] Laboratory of Computational and Structural Physical-Chemistry for Nanosciences and QSAR, Biology-Chemistry, Department, West University of Timisoara, Timisoara, Romania.
[3] Laboratory of Renewable Energies-Photovoltaics, National Institute for R&D in Electrochemistry and Condensed Matter INCEMC-Timisoara, Timisoara, Romania.
[4] Mesalands Community College, Tucumcari, NM, USA.
[5] Department of Computer Science, KU Leuven, Belgium.
* corresponding authors: ottorino.ori@gmail.com, mv_putz@yahoo.com.

croscopy measurements [1] allowing 1-Å resolution at an acceleration voltage of only 80 kV. The first direct imaging of *formation and annealing* process of various defects of both natures, topological (like Stone-Wales rotationdefectsm in short SW) and structural (single and double vacancies, vacancy clusters, adatoms, grain boundaries, etc.), we have made immediately clear the importance of exploring the dynamics of graphene imperfections which largely influence electronic, thermal and mechanical properties of hexagonal nanosystems. In particular, reference [1] illustrated the fast elimination of a Schottky single-vacancy defects involving one reconstructed pentagon, which returned to the pristine honeycomb status after the missing atom was replaced by an extra-carbon atom diffusing on the surface of the graphene sheet surface. Within the graphene basal plane, self-healing of vacancies is surely favored by the interactions among π-π orbitals which stabilize the 2D-mesh of sp^2 carbon atoms. Normally in fact, high concentrations of vacancy defects in graphene occurs only when energy processes are involved, such as neutron or ion bombardment, electronic irradiation, or after atomic-scale should help in modeling graphene band-prperties such as the appearance of loxalized electron states near the Dirac point in case of vacancies. Structural and topological defects, by altering in a profound way graphene's performances, prompt scientists for a detailed description of the mechanisms governing their formation and evolution. Recently, theoretical instigations on the evolution of multiple vacancies in graphene based on *nonequilibrium molecular dynamics* [5], provided strong evidence system tendency toward large holes as the number of vacancies N_v increases. For lower N_v, haeckelite-like structures are hoverer present, the number of pentagon–heptagon pairs growing linearly with N_v. Such a linear relationship has been interpreted as the consequence of the (tentative) compensation of the missing area around the N_v missing atoms which preserves, at the same time, the sp^2 network. After self-healing, the percentage of non-hexagonal rings in the graphenic sheet results six times the number of missing atoms, approximately. Other studies [5] report about quantitative description, based on DFT calculations, of the formation mechanism of amorphous graphene under electron irradiation, still confirming the importance played by electronic processes leading to the reconstruction of lattice regions also when multiple vacancies are initially present.

Present research mainly indicates that *the self-healing featured by defective honeycomb networks, corresponds to an universal topological feature arising from the topology of the 3-connectd hexagonal network treated as a whole* — an agile technical definition of these concepts is provided by following chapter – rather than an effect arising from the fine tuning of DFT detailed. somehow arbitrary parametrizations. That topological property applies therefore to defective graphene sheets and to general honeycomb lattices when other elements other than carbon are present. Graphene, in interaction with various heteroatoms or molecules, offer infinite freedom to design nano-devices [6]. Ab-initio characterization of vertical heterostructures made of graphene, metal substrates and intercalated of heteroatoms evidenced for the first [7] time the crucial role of non-local *cooperative interactions between heteroatoms, graphene, and substrate.* By combining

scanning tunneling microscopy measures with density functional theory, the Si intercalation process between graphene and Ru(0001) is described in [7] as a 4-steps mechanism involving i) defects creation; ii) migration of heteroatoms; iii) honeycomb carbon network self-heal; iv) growth of intercalated monolayers. Other combinations of heteroatoms (Ni, Pd, Pt) and substrates (Ir(111) and SiC(0001)) have been also analyzed, supporting the generality of the study. Theory and experiments both agree this 4-steps mechanism applies to different [hetero-atoms — substrate] combinations, suggesting that it comes, more likely, from *inherent topological properties of honeycomb lattices.*

Intriguingly, authors claim [7] that "We find that heteroatoms, graphene, and substrate need to be considered as a whole in order to understand the intercalation process", that is exactly what arises from present topological simulations:

- *Topology therefore emerges like the driving force guiding the cooperative evolution of honeycomb systems with structural defects toward stable configurations.*

Whereas topo-thermodynamic investigations have been already applied to determine the evolution of topological potentials in defective graphenic and metallic systems [8,9], this work provides more details about the non-local mechanisms which promotes the probability of formation of clusters of vacancies in graphenic lattices with N_C carbon atoms and N_v vacancies. Our topological modeling (TM) techniques reveal in fact the existence of a peculiar *topological cooperative* accumulation of vacancies in honeycomb lattices, by exhibiting a ladder-like behavior which dominates, in a nontrivial way, both genesis and evolution of vacancies clusters and appears to be of critical importance in the effort to establish the proper design-rules for graphene-based new materials.

Next paragraphs are devoted to elucidate the essence of the TM approach, with a short digression on the concept of *topological efficiency*, the lattice descriptors that allows detailed and methods for simulating periodic graphenic systems with N_C carbon atoms and N_v vacancies mutually interacting being the number N of hexagonal sites $N = N_C + N_v$ precisely conserved. TM results will be then presented and discussed in details, and a comparison with literature finding about *self-healing mechanisms* in graphene will be finally reported.

2 The topological picture

In graphene, long-range interactions basically derive from the delocalized nature of the π-electron belonging to the tree-folded sp^2 hybrid orbitals of the carbon atoms constituting the honeycomb mesh. In turn, the changes in the electronic structure strongly depend on detailed

characteristics of the defects, like the presence of dandling bonds, and possible saturation or reconstruction in the case of vacancies [10]. The stabilizing role played by *long-range potentials* has an indubitable topological origin as demonstrated by previous simulations on graphenic lattices featuring the presence of sequences of Stone-Wales linear defects, or SW waves [11]. Original results in [11] also suggest the topological origin at the basis of the *inherent anisotropy* exhibited in graphene fragments by many physical effects connected to electronic transport properties. According to the topological picture adopted here, the *long-range* nature of the topological potentials Ξ is originated by the dependence on the $(N^2 - N)/2$ independent elements $\{d_{ij}\}$ of the symmetric, zero-diagonal, distance matrix $\hat{D}(G)$

$$\hat{D}(G) = \begin{bmatrix} 0 & d_{12} & \cdots & d_{1N} \\ d_{21} & \ddots & & \vdots \\ \vdots & & \ddots & d_{N-1,N} \\ d_{N1} & \cdots & d_{N,N-1} & 0 \end{bmatrix} \tag{1}$$

Operator $\hat{D}$ fully represents honeycomb system under study which is depicted as a 3-connected chemical graph G with N vertices and number of pristine bonds scaling like $3N/2$.

Any topological potential Ξ constructed on the $\{d_{ij}\}$ set behaves as a *long-range potential* and may be usefully applied for simulating chemical structures in which every atom interacts with all the remaining ones. In this way, long-range interactions induced by ı-orbitals are theoretically investigated by adopting a topological potential Ξ which represents a valid alternative to parametrized DFT methods for preliminary fast simulations of graphenic systems with vacancies. TM techniques simply rely on schematic representations of molecules and lattices in terms of the so-called *chemical graph* $G(N, E)$ with N nodes (atoms) connected by E edges (chemical bonds). As stated above, topological graphs are *completely* described by the information stored in their distance matrix Eq(1) or, more precisely, in their adjacency matrices $\hat{A}$, that is still a $N \times N$ symmetric operator just counting chemical bonds, being $a_{ij} \neq 0$ only if atoms i and j are connected, in which case $a_{ij} = 1$. These sparse matrices have exactly $2E$ entries equal to 1.

The 3-connected graphene sheet is conveniently described by a planar *cubic* (trivalent) graph with N-vertices covering a certain number of hexagonal carbon rings. Following TM approach, a given chemical system evolves in such a way certain *distance-based topological invariants* Ξ to reach their minimum. By sorting the chemical distances d_{ij} the following definition of its Wiener-weight w_i is derived:

$$w_i = \frac{1}{2}\sum_{j=1}^{N} d_{ij} = \frac{1}{2}\sum_{k=1}^{M_i} k b_{ik}. \tag{2}$$

In (2) b_{i1} is the number of the k-shell of node i. In a general nodes exhibit different eccentricities M_i being graph diameter $M = \max\{d_{ij}\} = \max\{M_i\}$ and graph radius $m = \min\{M_i\}$, normalization constraint $N - 1 = \sum_k b_{ik}$ being valid for any atom i. In fullerenes and periodic nanographene fragments all nodes show $b_{i1} = 3$ the signature of ideal sp^2 hybridization. The sum of all Wiener-weights produces the Wiener index W that measures of the *topological compactness* of the structure:

$$W = \sum_{i=1}^{N} w_i \tag{3}$$

Symmetry equivalent atoms share the *same* set $\{b_{ik}\}$ (the converse is not true). For example $C_{60} - I_h$ fullerene atoms share the invariants $\{b_{ij}\} = \{3, 6, 8, 10, 10, 10, 8, 3, 1\}$, $M = 9$ and $w_i = 139$. Eq(2,3)yield to $W = 8340$ for Buckminsterfullerene (see original computation in 1992 article [13]). Invariants in (2) are instrumental to expresses the long-range effects induced on atom i by overall topological structure of the graph.

For graphene, Figure 1 gives the periodic super-cell adopted in the following having $N^{(0)} = 800$ atoms $n_x \times n_y = 200$ cells, with $n_x = 10$ and $n_y = 20$. Also this pristine graph $G^{(0)}$ is highly symmetrical, being all nodes symmetry-equivalent with 40 coordination shells ($M^{(0)} = 40$), $\{b_k^{(0)}\} = \{3\ 6\ 9\ 12\ 15\ 18\ 21\ 24\ 27\ 29\ 29\ 28\ 27\ 26\ 25\ 24\ 23\ 22\ 21\ 20\ 20\ 20\ 20\ 20\ 20\ 20\ 20\ 20\ 20\ 2020\ 20\ 20\ 20\ 20\ 20\ 20\ 20\ 20\ 10\}$; $w_i = 8,330$ with $W^{(0)} = 6.664,000$. For an open (e.g. non periodic) fragment, carbon atoms along the edges show higher w_i values suggesting the *approximate proportionality* between w_i value and relative reactivity. Focusing on this property of the Wiener-weights Eq(2), specific topological invariants targeting the measure of the topological efficiency of G have been introduced [16,17], showing a pivotal role in selecting stable configurations of the chemical system also in presence of defects [14-18].

Topological efficiency descriptors may be defined starting from the properties of the so-called minimal $\underline{V}$ and maximal vertices $\overline{V}$ of the G featuring $\underline{w}$ and maximal $\overline{w}$. Heuristically one may assign to $\underline{V}$ or $\overline{V}$ the role of the most or less stable atoms in the chemical graph respectively. Minimal $\underline{w}$ and maximal $\overline{w}$ are computed according to the following definitions

$$\underline{w} = \min\{w_i\}, \quad \overline{w} = \max\{w_i\}, \quad i = 1, 2, \ldots, N-1, N. \tag{4}$$

Minimal (maximal) vertices provide the lowest (highest) contributions to Wiener index (3). Minimal nodes furthermore correspond to the nodes with the deepest embedding in G, highly contributing in such a way to the topological compactness of G. The graph G is *topologically efficient* when the remaining atoms behave in a comparable way, e.g. when terms w_j have values closed to $\underline{w}$. Two recent invariants rank very well the topological efficiency (also called topological roundness) of a set of a similar structures like isomers or defective lattices; they are

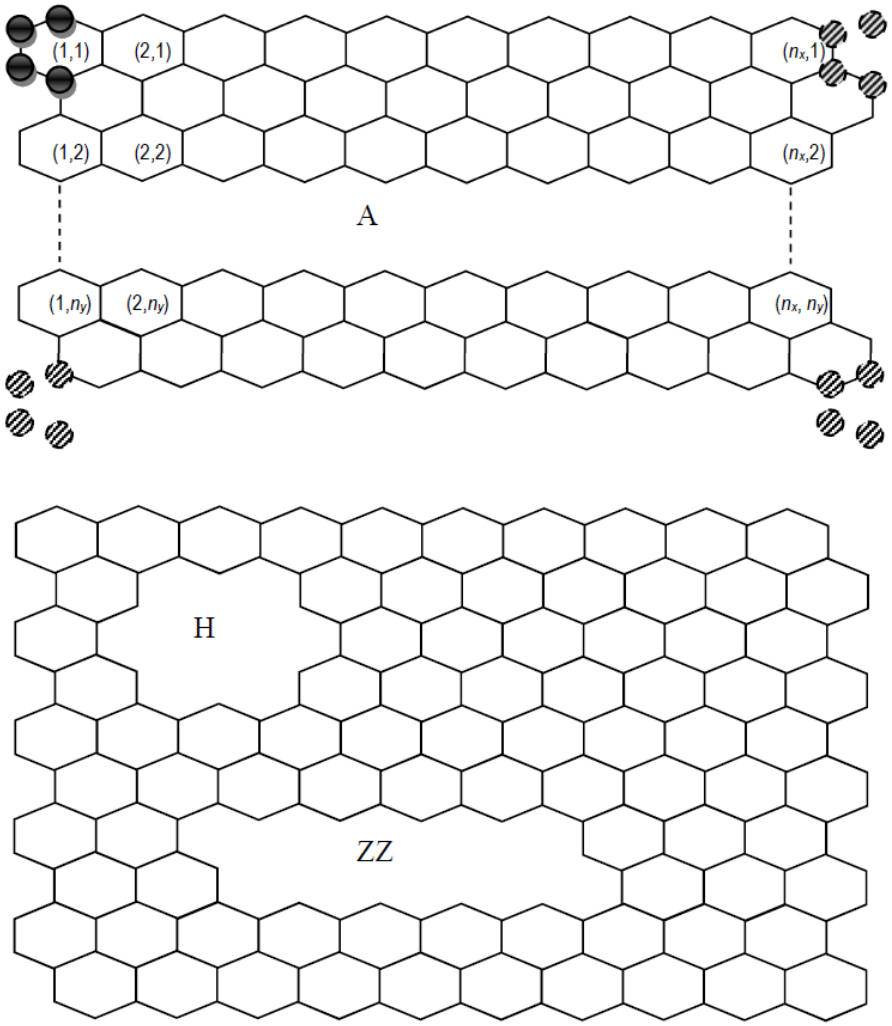

Fig. 1. (A) The super-cell $G^{(0)}$ considered in this work includes $n_x \times n_y$ unit cells ($n_x = 10, n_y = 20$) with $N = 800$ honeycomb sites; unit cell has 4 atoms (black); periodic conditions are indicated by shaded balls. (B) region with a vacant hexagonal ring with 6 dandling bonds. (ZZ) linear vacancies forming a reactive region.

defined as follows:

$$\rho = W/Nw, \quad \rho > 1 \tag{5}$$

$$\rho^E = \overline{w}/\underline{w}, \quad \rho^E \geq 1. \tag{6}$$

Above topological indices are known as *topological efficiency index* ρ (5) and *extreme topological efficiency index* ρ^E (6) respectively [16,17], and both tend to favor chemical networks with a compact structure built around their minimal sites. TM simulations based on the minimization of topological potential $\Xi^{\rho} = \rho$ and $\Xi^{\rho E} = \rho^E$ show good correlations with molecular stability data, as demonstrated by extensive studies on C_{28}, C_{50}, C_{66} fullerenes and defective honeycomb layers [11,14-18].

In this paper the *extreme topological efficiency* invariant $\rho^E(G)$ has been chosen as lattice topological potential $\Xi(G)$:

$$\Xi(G) = \rho^E(G). \tag{7}$$

Topological potential (7) is able to simulate long-range interactions in graphenic systems at a very low computational cost. Moreover, obeying to the minimum-principle mentioned above, it drives the evolution of the graph G with vacancies evidencing remarkable effects on the concentration of the vacancies itself as the next paragraph will show.

3 Toplological modelling results

Considering the periodic pristine honeycomb $G^{(0)}$ with $N^{(0)} = 800$ atoms of in Figure 1A, the evolution of the graphenic layer is simulated by computing the *topological potential* $\Xi(G)$ (7) as a function of the growing number N_v of vacancies *randomly* placed in the mesh. The concentration of vacancies is indicated by the symbol $c_v = N_b/N^{(0)}$. In order to define the correct scope of topological simulations, it is important to remembering that:

- TM *approximate* methods are aimed to compare chemical structures made with similar building units, in this case this condition is assured by limiting vacancies concentration $c_v < 15\%$.
- The *periodic conditions* applied on $G^{(0)}$ make this system perfect for modeling vacancy effects on *graphene basal plane*.

Periodic graphene $G^{(0)}$ features a highly symmetric configuration $\rho^E = 1$ being all nodes interchangeable $w^{(0)} = w_i = 8,330$. When the first vacancy is placed in the lattice (Figure 2), topological invariants show typical variations which are unaffected by the specific selection of the removed atom: the Wiener index of the defective lattice $G^{(1)}$ with $N_v = 1$ and $N = 799$ decreases to value $W^{(1)} = 6,648,716$ as the lattice loses the initial honeycomb symmetry, with a "cascade" of different w_i entries produced by Eq.(2), which is able to differentiate the $N^{(1)}$ atoms on the basis of the populations in their coordination shells $\{b_{ik}\}$. Three nodes in $G^{(1)}$ present one dandling bonds and for this reason have the highest value w_i; they are grouped in 2 sets, named A and B in Figure 2, with topological descriptors as follows. Atom A has

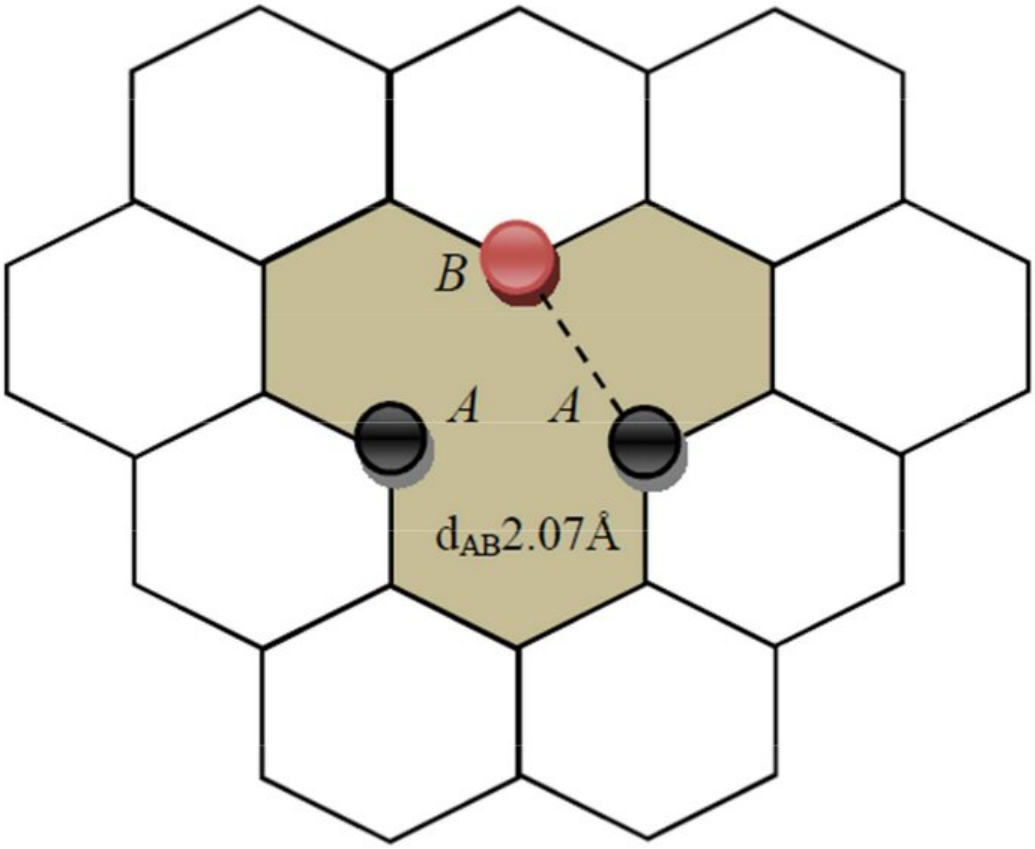

Fig. 2. Monovacancy in graphene: atoms with dandling bonds $b_1 = 2$, two A and B, and highest Wiener-weights $w_A = 8382.5$ and $w_B = 8637.5$ are topologically the most reactive sites of the nanographenic layer; A-B bond reconstruction is an allowed mechanism from both chemical and topological rationals.

$w_A = 8382.5$, $\{b_{Ak}\} = \{2\ 4\ 7\ 11\ 14\ 17\ 20\ 23\ 26\ 29\ 30\ 29\ 28\ 27\ 26\ 25\ 24\ 23\ 22\ 21\ 20\ 20\ 20\ 20\ 20\ 20\ 20\ 20\ 20\ 20\ 20\ 20\ 20\ 20\ 20\ 20\ 20\ 20\ 20\ 20\ 20\ 20\ 10\}$ keeping 40 coordination shells like for the atoms of the pristine graphene $G^{(0)}$. Atom B represents the maximal node of $G^{(1)}$ with $w_B = \overline{w} = 8637.5$ showing an extra 41th–coordination shell with 10 atoms in its string $\{b_{Bk}\} = \{\ 2\ 4\ 7\ 11\ 14\ 17\ 20\ 23\ 26\ 28\ 28\ 27\ 26\ 25\ 24\ 23\ 22\ 21\ 20\ 20\ 20\ 20\ 20\ 20\ 20\ 20\ 20\ 20\ 20\ 20\ 20\ 20\ 20\ 20\ 20\ 20\ 20\ 20\ 20\ 20\ 10\}$. A and B share the same number $b_{A1} = b_{B1} = 2$ of first-neighbors and similar populations on the first 10-coordination shells. For $k \geq 11$, entries are different $b_{Ak} \neq b_{Bk}$ and the two sites become *topologically distinct*, violating in such way the local triangular symmetry some researchers quote [19].

According with TM, the highest w_i is the reactivity of the i-atom, then carbon atoms A and B are topologically (and chemically) the most reactive ones with $\overline{w} = w_B > w_A$. Bond reconstruction inside the hole caused by the monovacancy in Figure 2 should then go — for pure topological reasons — from atom B to A, being this topological prediction confirmed by *ab-initio* calculations based on density functional theory [20]. Although the presence of monovacancy $N_v = 1$ does not change the structure of the defective lattice $G^{(1)}$ too much, both the minimal and maximal Wiener-weights are quite sensible lattice descriptors assuming the new values $\underline{w} = 8310$ and $\overline{w} = 8637.5$ respectively. From Eq.(6), the topological efficiency value $\rho^E = 1,0394$ is computed for $G^{(1)}$; this value is greater than $\rho^E = 1$ of pristine $G^{(0)}$, stating in such a way that the *network topology* and the topological potential $\Xi(G)$ (7), *obstacle the creation of a monovacancy.*

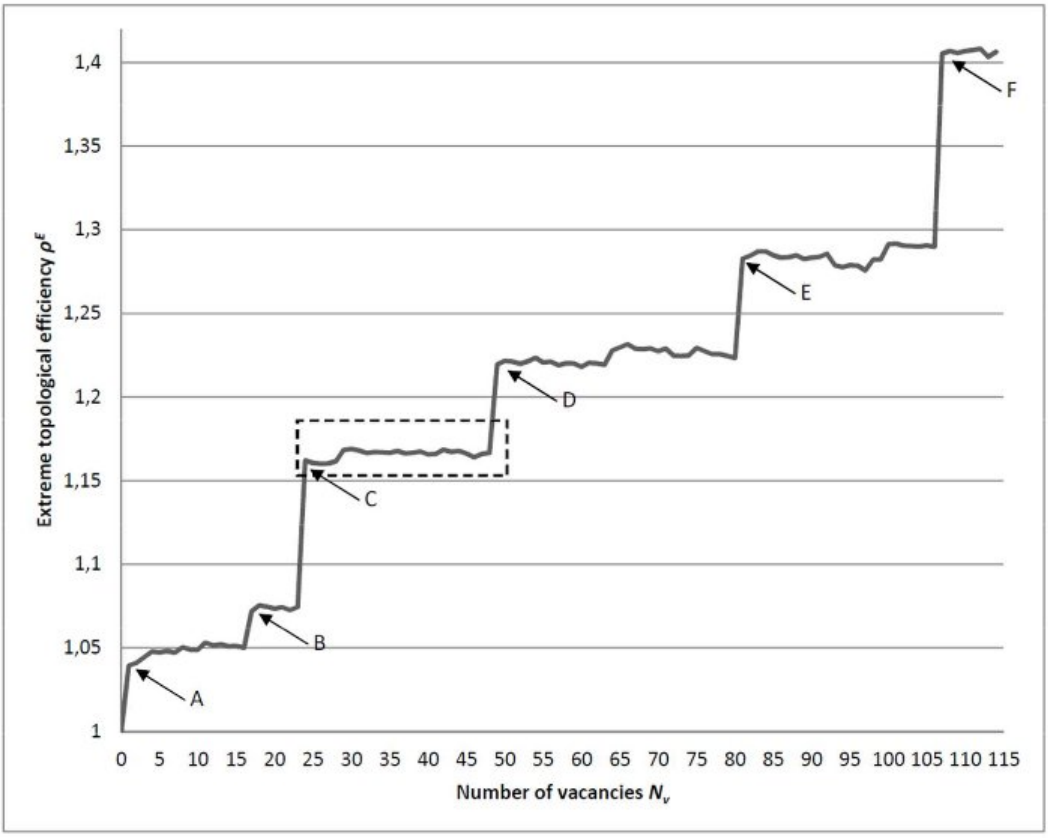

Fig. 3. The curve for ρ^E in graphene with N_v vacant atoms; characteristic steps evidence the formation of vacancy clusters: first vacancy formation $N_v = 1$ (A) ; 6-ring looses 3 (or 4 or 5) bonds with typical barriers (B or C or E); the curve jumps also when other 6-ring looses 5 bonds (D) or during the formations of extended linear defects (F). Dashed inset evidences a flat ρ^E region in which vacancy clusters are therefore generated without topological obstacles.

When the number of vacancies increases up to $N_v = 114$, their concentration varies in the $0\% \leq c_v \leq 14.25\%$ interval, the variations of the topological potential ρ^E are easily computed and some very interesting mechanism often emerge from random topological simulations.

Figure 3 illustrates the typical *ladder-like curve* describing the evolution of ρ^E in the defective honeycomb lattice for $0 \leq N_v \leq 114$. In pristine graphene at ambient temperature, the formation energy E_f of a single Schottky vacancy $E_f = 7.9$eV and the energy 4.9eV of a single bond $C - C$ (1.42Å) both contribute to determine the equilibrium vacancy [20]. E_f value, corresponding to the first step in the ρ^E curve, may be used to determine the energy scale of the ρ^E curve itself (Figure 3A). As mentioned, the three dangling bonds surrounding the vacancy tends to form one reconstructed bond with length of 2.07Å (Figure 2) that has to be compared to the 2nd-neighbors distance 2.46Å in pristine honeycomb [20]. These forms of reconstructed structures are not considered in the current TM study.

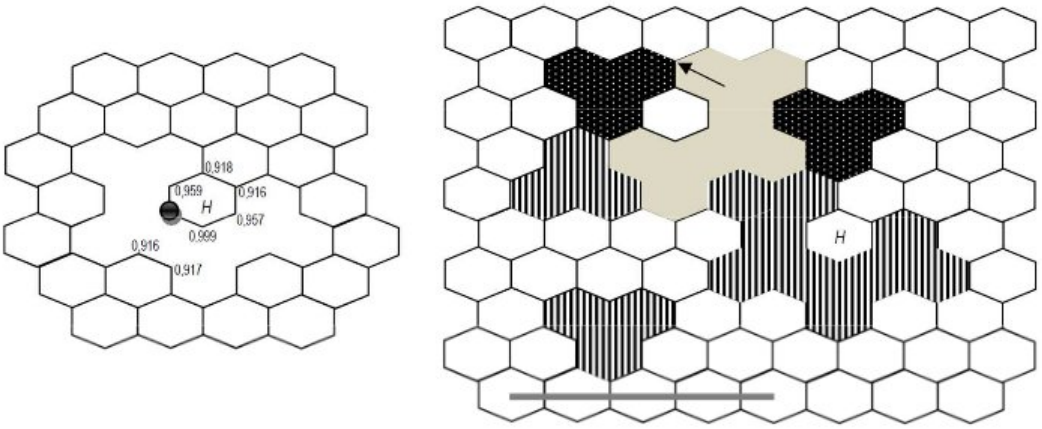

Fig. 4. Left: vacancy cluster surrounding a benzenoids ring H with 4 dandling bonds forming a large topologically reactive region corresponding to Figure 3C configuration. Atom with black ball has the largest topological reactivity with $\overline{w} = 9355$; for some atoms $w_i/\overline{w}$ ratio is reported to measure relative reactivity. Right: the region after the insertion of other vacancies around a second benzenoids R, just before cutting a 5th R bond by removing the arrowed node causing Figure 3D jump (1nm bar is reported for convenience).

After the first *repulsive* jump that corresponding to the creation of the first vacancy (Figure 3A), of the topological potential $\Xi(G)$ (7) corresponding to the creation of the first vacancy (Figure 3A), the systems admits the creation of new vacancies keeping the topological potential (7) curve *substantially flat*. The situation varies, with a sharp increase in ρ^E, when one of the hexagonal ring loses 3 (and then 4) bonds connecting it to the lattice, creating respectively the

arrowed steps B and C in the ρ^E curve. The random generation of vacancies creates typical defective cluster like the ones depicted in Figure 4 with just 2 edges bridging the pruned hexagon H to the rest of the honeycomb graph. In these highly defective regions the reactivity hierarchy of the involved atoms is again effectively ranked by the w_i atomic entries: atoms belonging to the benzenoid H are the most reactive ones, including the 2 vertices in Figure 4 still with 3 bonds and relative Wiener-weight of 0.918 and 0.916 respectively. It is worth to evidence once more the ability of TM to produce *fast* and *accurate* reactivity maps of the graphenic atoms.

ρ^E descriptor encounters then a forth step Figure 3D when a second ring R, close to H, remains with just one bond connecting it to the graphenic layer. It's very interesting to observe that the graphenic system, after each ρ^E step in Figure 3, is allowed by the topological potential $\Xi^{\rho E}$ (7) to *accumulate* new vacancies keeping the topological potential practically constant in certain ranges of vacancy concentration, leading to a ladder-like, typical process of *vacancy accumulation*. See for example in Figure 3 the 3C-3D plateau corresponding to the $24 \leq N_n v \leq 47$ interval in which the topological potential $\Xi^{\rho E}$ remains flat, approximately at the $\rho^E_{(N_v=24)} = 1.1621$ level *although vacancy concentration almost doubles* by passing from 3% to 5.9%, forming nanometric-sized defective regions in the lattice (see Figure 4). According to [21], such a kind of large *randomly oriented* clusters of vacancies may lead to *graphene amorphization* and largely influenced by the electronic features of the carbon atoms and the chemical dopants possibly present. Lattice descriptor ρ^E sharply grows when also hexagon H remains with a single dandling bonds (Figure 3E step) and new multiple vacancies (Figure 3F step) are distributed along quasi-linear configurations in the layer. According to the present model, quasi-linear configuration of vacancies are disfavored by the topological potential $\Xi^{\rho E}$ barrier and appear for such a reason topologically less stable than the typical cluster-like defects represented in Figure 4. Similar clusters have been *experimentally documented* [7], by STM high-resolution images concerning Si-intercalated graphene grown on Ru(0001) confirming the morphological predictions of TM computations which are able to simulate such kinds of nano-sized clusters like the one represented in Figure 5. In [7] authors introduce cooperative interactions between heteroatoms, graphene, and substrate, involving creation of vacancies, heteroatoms migration, graphene self-healing. These cooperative mechanisms are proposed having a crucial role in driving the growth of vertical heterostructures including the observed self-reconstruction of the pristine honeycomb carbon lattice, with the removal of vacancies in the temperature range 300-800°C. Present results, based on numerical simulations of the topological potential $\Xi^{\rho E}$ provide more insights on the roots of cooperative interactions in graphenic systems, by highlighting as a key factor the *long-distance topological structure of the honeycomb lattice itself*. Self-repair of the graphene lattice is confirmed y several studies of multiple vacancies in graphene and graphene nanoribbons explored by quantum calculations predicting hole annihilation [22,23,24]. Being the $\Xi^{\rho E}$ curve totally *reversible* in the quasi-flat regions represented in in Figure 3, the possibility to close the holes at zero-cost in topological energy is an

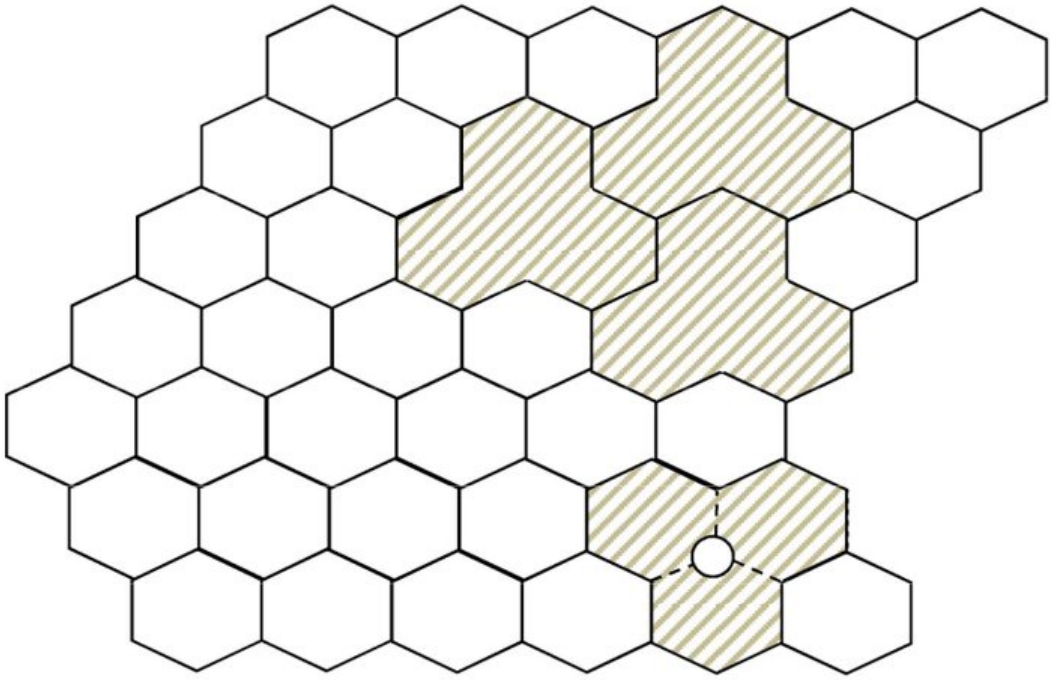

Fig. 5. Typical cluster-like accumulation of vacancies in graphene as pictures by STM data; here 4 vacant atoms generate holes in a quite dense configuration (one of vacant node is represented with a circle).

immediate consequence of the present model, making also the self-healing a mechanism which is allowed by *long-range topological structure* of the honeycomb lattices. Self-healing mechanisms of vacancy defects in hexagonal planes different from graphene and therefore possible, from a topological perspective, also in chemical structures with a lack of sp^2 interacting orbitals, like silicone. Recent studied on silicene using first-principles calculations [25] confirm the reconstruction of the single vacancy through the (nonmagnetic) sp^3 coordination of atoms surrounding the vacancy. In general, for honeycomb lattices made of elements (like Si, Ge, etc) other than carbon, one has to define which kind of long-range electronic interactions may take the place of the sp^2 orbital interactions. A possible answer to this question is related to the presence in the honeycomb lattice of bondons $\mathcal{B}$, the bosonic relativistic quasi-particles dually connected to the chemical bond fields. As reported in the innovative study [1]) on graphenic 1D nanoribbons, at the typical space-scale of 15–30 Å, long-range bonding interactions arise from the action of these new particles, which are then able of inducing cooperative phase-transitions in hexagonal systems with low dimensionality. The role of Stone-Wales topological defects in healing silicene vacancy is also evidenced [25] confirming in such a way previous topological simulations [26] about the effects of Stone-Wales topological isomerisations on bondonic

states in 1D honeycomb nanoribbons made of Si, Ge (germanene), Sn (stannene) and hetero-combinations of Group-IV elements. It's worth noticing that [25] provide a correct ab-initio descriptions of the *asymmetric* reconstruction of the single vacancy in graphene driven by the magnetization acquired during dangling bons rebonding. Bondons induce phase-transitions on low-dimensions systems, with specific space-, time- and bond energy-scale, providing in such a way a peculiar form of long-range inter-atomic interaction which is universally present in honeycomb structures [26]. Bondons may help in fully understanding electronic and transport properties of honeycombs with vacancies, as shown in Figure 6 for nanoribbons. One may in fact firstly consider the correspondence among the topological levels of Figure 3 and the respective band-energy levels of the nanostructure in which a vacancy, being surrounded by dangling bonds which obstacle the circulation of the electronic charges, behaves as a *positive charge carrier*. Accordingly, the nanostructure with more vacancies will therefore possess a more distinguished p-type semiconductor behavior. Since part of the electronic bonds are cancelled in nanostructures with vacancies, *bondons* as the quantum pairs of electrons, and the respective bondoles (bonding-of-holes) constitute a network of quantum particles interacting, through the honeycomb mesh, with vacancies; as a note, standard excitions (electron-hole pairs) may be now generalized by so-called bondots (bonding-of-dots), particles arising from the interaction of bondons and bondoles.

Apart from these speculations on quantum exotic particles in honeycomb nanostructures with vacancies, we remain with the basic idea that honeycomb structures with certain concentrations of vacancies may be approached like p-semiconductor nanosystems; consequently, gradients in the local populations of vacancies in nanoribbons will create n-p homojunctions with associated photovoltaic effects and specific absorption coefficients. For the graphenic systems considered in this paper, it's also possible to identify the N_v values making the system more conductive (Figures 3 and 6). Our preliminary results indicate in fact that defective layers with configuration type A and D, having number of vacancies varying between 5-15 and 50-85 respectively, are excellent candidates for producing nanosystems with controlled (constant) thermal conduction.

Finally, interesting considerations on $\{b_{ik}\}$ populations are also derived by TM computations (see Figure 7). In pristine graphene $G^{(0)}$ the number of atoms on the $M^{(0)} = 40$ coordination shells characterizing pristine $G^{(0)}$ shows peaks in correspondence of $k = 10, 11$ both with 29 atoms providing in such a way the characteristic shape Figure 7A) In the left part of the histogram for $k = 1, 2, ...8, 9$ populations b_k are multiples of 3, followed by a linear descent and by an extended region including $M^{(0)}/2$ coordination shells ($k = M^{(0)}/2, M^{(0)}/2+1, ...M^{(0)}/2-2, M^{(0)}/2-1$) with a constant number of 20 neighbors. In the fairest shell $k = M(0) = 40$ the population suddenly drops to 10. The histogram in Figure 5 represents then the *topological fingerprint* of the ideal graphene lattice $G^{(0)}$ without vacancies. In order to determine analogous histogram for $n_y/2 \times n_y$ honeycomb lattices with different sizes (present size being $n_y = 20$) it

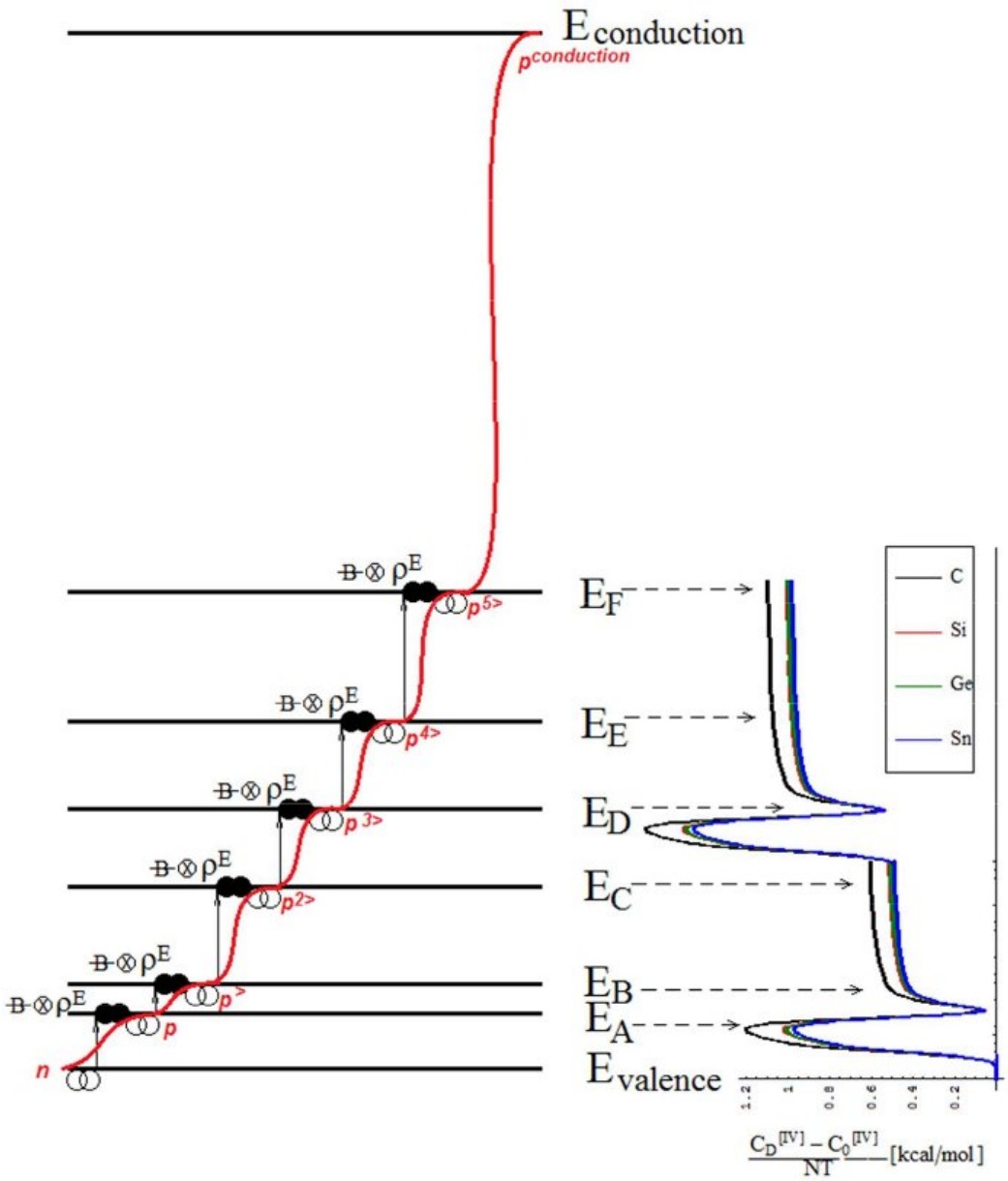

Fig. 6. The correspondence of the nanoribbons with vacancies of Figure 3 with the paradigmatic p-semiconductor, with successive intermediate layers of acceptor levels, along the bondonic forming as driven by the topological efficiency of the structures with larger and larger vacancies, paralleling the increase of p-doped character ($p < p^{>} < p^{2>} \cdots$), and the associate bondonic (B) signal in defect-to-pristine honeycomb lattices [26], respectively, for the IV group's nanostructures.

is worth noticing that $M^{(0)} = 2n_y$, and scale the results accordingly.

Viewed from the minimal node of $G^{(48)}$ lattice (Fig.7B), lattice $G^{(48)}$ which corresponds to the graphene layer with $N_v = 48$ vacancies just before the step-barrier in Figure 3D, the lattice keeps its graphenic nature only for the first $k = 1, 2, 3$ coordination shells and for a few other cases like $k = 40$. The vacancy concentration of about $c_v = 6\%$ forces the lattice adjust also its topological diameter (the longest chemical path) that increases from $M^{(0)} = 40$ to $M^{(48)} = 41$. This phenomenon gets enhanced in $G^{(49)}$ (Fig. 7C) after the insertion of an extra-vacancy which causes a sharp elongation of the diameter $M^{(49)} = 43$ and the connected sharp step in Figure 3D. The system is in fact forced to find longest paths to connect all atoms, increasing in such a way the importance of the coordination shells of higher orders.

Summarizing, present theoretical work on graphene vacancies specifically demonstrates that defect-generation and annihilation are both largely influenced by the long-range topological properties of the original hexagonal mesh; in particular Figure 3 shows that:

- *Vacancies accumulation effect* may be described — for certain vacancy concentration intervals — as an inherent *topological property* of the honeycomb networks mainly depending from the *ladder-type behavior* of ρ^E, the extreme topological efficiency descriptor defined by Eq(6);
- Within the concentration intervals in which index ρ^E remains quasi-flat, *reversible holefilling is allowed*, providing pure *topological roots to the graphene self-heal effect* experimentally reported;
- Moreover, the general presence of bondons in honeycomb networks, provides a *long-range inter-atomic* interactions generally applicable to graphene layers ad other hetero-combinations of Group-IV elements.

Future work will be devoted to correlate the influence of lattice point defects (like chemical impurities and vacancies) and bondonic states on the electronic transport properties of graphenic systems and PAH's.

4 Conclusion

Topological efficiency invariants evidence the importance of long-range topological interactions in explaining the properties of graphenic layers; in particular present results establish in great details some interesting [topology / defects] correlations, which appear to be of some importance for the novel graphene nanoscale science. The lack of (topological) energy barrier in augmenting the number of vacancies at certain vacancies concentrations values and the typical ladder-like curve (Figure 3 has been derived here showing that in certain condition, *the long-range*

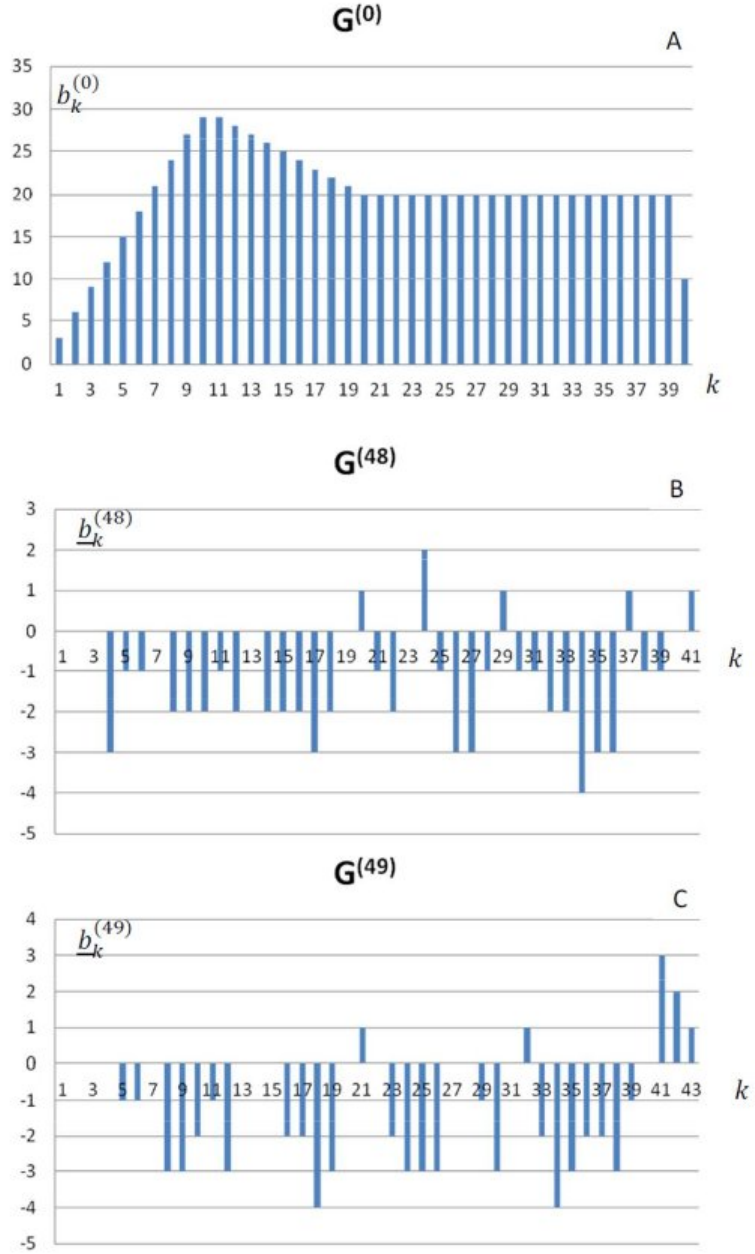

Fig. 7. The populations $\{b_{ik}\}$ of the coordination shells of the minimal nodes for graphene lattice $G^{(0)}$ (A) and defective layers $G^{(48)}$ (B), $G^{(49)}$ (C). In $G^{(0)}$ all nodes have the same set $\{b_{ik}\} = \{b_k^{(0)}\}$; differences $b_k^{(48)} - b_k^{(0)}$ are instead represented for the minimal nodes of $G^{(48)}$ and $G^{(49)}$ graphs. Topological diameters are $M^{(0)} = 40$, $M^{(48)} = 41$ and $M^{(49)} = 43$.

connectivity features of the honeycomb networks allow vacancy accumulation and annihilation in nanographene and, more in general, in honeycomb structures.

Furthermore, the presence of delocalized bondonic states provide universal long-range electronic interactions able to guarantee the appearance of vacancy accumulation and self-healing effects in graphene and non-carbon honeycomb systems. Remarkably, the bondonic predicts the level of vacancy concentration that allows to acquire a semiconductor-like effect that may be detected via thermo-conductivity and photovoltaic measurements. Further topological, bondonic and experimental studies will carried out to provide more details on the theoretical mechanisms proposed here, involving single- and multiple-layers of graphene, graphene-silicene combinations, heterojunctions with photovoltaics materials with possible applications in domains sich as nanoelectronics, thermal and electrical high-conductivity devices and renewable energies.

5 References

[1] Meyer J.C., Kisielowski C., Erni R., Rossell M. D., Crommie M.F., Zettl A. (2008). Direct Imaging of Lattice Atoms and Topological Defects in Graphene Membranes, *Nano Letters*, **8**(11), 3582-3586, doi: 10.1021/nl801386m

[2] (a) Satuła, W., Dean, D. J., Gary, J., Mizutori, S., Nazarewicz, W. (1997). On the origin of the Wigner energy. *Physics Letters B*, **407**: 103-109. (b) Ewels, C. P., Telling, R. H., El-Barbary, A. A., Heggie, M. I., & Briddon, P. R. (2003). Metastable Frenkel pair defect in graphite: Source of Wigner energy? *Physical Review Letters*, **91**: 025505

[3] (a) Cataldo F., (2000) A Raman study on radiation-damaged graphite by γ-rays. *Carbon*, **38**: 634-636. (b) Cataldo F., Ursini O., Nasillo G., Caponetti E., Carbone M., Valentini F., Braun, T. (2013). Thermal properties, Raman spectroscopy and TEM images of neutron-bombarded graphite. *Fullerenes, Nanotubes and Carbon Nanostructures*, **21**, 634-643. (c) Cataldo F., Angelini G., Révay Z., Osawa E., Braun T. (2014). Wigner energy of nanodiamond bombarded with neutrons or irradiated with γ-radiation. *Fullerenes, Nanotubes and Carbon Nanostructures*, **22**, 861-865. (d) Cataldo F., Iglesias-Groth, S., Hafez, Y., Angelini, G. (2014). Neutron bombardment of single wall carbon nanohorn (SWCNH): DSC determination of the stored Wigner-Szilard energy. *J. Radioanal. Nuclear Chem.* **299**: 1955-1963.

[4] (a) Cataldo F., Baratta G. A., Strazzulla, G. (2002). He+ ion bombardment of C60 fullerene: An FT-IR and Raman Study. *Fullerenes, Nanotubes Carbon Nanostruct.* **10**: 197-206. (b) Cataldo F., Baratta G. A., Ferini G., Strazzulla G. (2003). He+ Ion Bombardment of C_{70} Fullerene: An FT-IR and Raman Study. *Fullerenes, Nanotubes and Carbon Nanostructures*, **11**, 191-199. (c) Xu, Z., Chen, L., Zhou, B., Li, Y., Li, B., Niu, J., Qian, X. (2013). Nano-

structure and property transformations of carbon systems under γ-ray irradiation: a review. *RSC Advances*, **3**: 10579-10597.

[5] Zhao R., Zhuang J., Liang Z., Yan T. and Ding F. (2015) The formation mechanism of multiple vacancies and amorphous graphene under electron irradiation, *Nanoscale* doi: 10.1039/c5nr 00552c

[6] Britnell, L.; Gorbachev, R.V.; Jalil, R.; Belle, B.D.; Schedin, F.; Mishchenko, A.; Georgiou, T.; Katsnelson, M.I.; Eaves, L.; Morozov, S.V.; Peres, N.M.R.; Leist, J.; Geim, A.K.; Novoselov, K.S.; Ponomarenko, L.A. (2012) Field-Effect Tunneling Transistor Based on Vertical Graphene Heterostructures. *Science*, **335**, 947-950. doi: 10.1126/science.1218461.

[7] Geng Li, Haitao Zhou, Lida Pan, Yi Zhang, Li Huang, Wenyan Xu, Shixuan Du, Min Ouyang, Andrea C. Ferrari and Hong-Jun Gao, Role of Cooperative Interactions in the Intercalation of Heteroatoms between Graphene and a Metal Substrate, *J. Am. Chem. Soc.* 2015 **137**, 7099-7103

[8] Ottorino Ori, Franco Cataldo, Mihai V. Putz IGI Entropy of Nanostructures. Topological Effects on Schottky Vacancies Concentration in Graphenic Bidimensional HC(N) Lattices, in *Sustainable Nanosystems Development, Properties, and Applications*. Eds. Putz M.V, Mirica M., IGI Global, Hershey, USA; in press.

[9] Kaatz, F; Bultheel, A.; Ori, O., Kinetic Monte Carlo Approach to Schottky Defects in Noble Metal Nanoclusters. Submitted to Nanotechnology, 2015

[10] T.M. Radchenko, V.A. Tatarenko, I.Yu. Sagalianov, Yu.I. Prylutskyy, G.V. Kurdyumov, Configurations of Structural Defects in Graphene and their Effects on its Transport Properties, in *Graphene, Mechanical Properties, Potential Applications and Electrochemical Performance, Series: Chemistry Research and Applications*, Editor B.T. Edwards, Nova Science Publishers, Inc., 2014 ISBN: 978-1-62948-796-0.

[11] Ori, O.; Cataldo, F.; Putz, M.V., Topological Anisotropy of Stone-Wales Waves in Graphenic Fragments. *Int. J. Mol. Sci.* 2011, **12**, 7934-7949.

[12] Putz M.V.; Ori O. (2012) Bondonic characteriza tion of extended nanosystems: Application to graphene's nanoribbons, *Chemical Physics Letters* **548** 95–100, doi: 10.1016/j.cplett.2012.08. 019

[13] Ori O.; D'Mello M. (1992) A topological study of the structure of the C_{76} fullerene. *Chemical Physics Letters*, **197**(1,2), 49-54

[14] Vukicevic D., Cataldo F., Ori O., Graovac A.(2011) Topological efficiency of C_{66} fullerene. *Chemical Physics Letters*, **501** 442-445.

[15] Iranmanesh, A.; Ashrafi, A.R.; Graovac, A.; Cataldo, F.; Ori, O., Wiener Index Role in Topological Modeling of Hexagonal Systems-From Fullerenes to Graphene, in: *Distance*

in Molecular Graphs Applications, Editors Gutman, I.; Furtula, B. University of Kragujevac, Kragujevac 2012 Mathematical Chemistry Monographs, Vol. 13, 135-155, ISBN:978-86-009-015-9.

[16] Ori, O ; Cataldo, F ; Graovac, A (2009) Topological Ranking of C_{28} Fullerenes Reactivity. *Fullerenes Nanotubes And Carbon Nanostructures*,**17**(3), 308-323. doi: 10.1080/15363830902782332

[17] Cataldo, F ; Ori, O ; Iglesias-Groth, S (2010) Topological lattice descriptors of graphene sheets with fullerene-like nanostructures. *Molecular Simulation* **36**(5), 341-353 doi: 10.1080/08927020903483262

[18] A. Graovac, A. R. Ashrafi, O. Ori: Topological efficiency approach to fullerene stability – Case study with C_{50}. *Advances in Mathematical Chemistry*, Vol. **2**, 2014, 3-23 Edited by S. C. Basak, G. Restrepo, J. L. Villaveces,; Bentham Science Publishers.

[19] Lehtinen O, Tsai I-L, Jalil R., Nair R.R., Keinonen J, Kaiser U, Grigorieva I.V., Non-invasive transmission electron microscopy of vacancy defects in graphene produced by ion irradiation, *Nanoscale*. 2014 Jun 21;**6**(12):6569-6576. doi: 10.1039/c4nr01918k.

[20] Paz W.S., Scopel W.L., Freitas J.C.C. (2013) On the connection between structural distortion and magnetism in graphene with a single vacancy. *Solid State Communications;* 171-176, 71-75.

[21] Pokropivny, A. V., Ni, Y., Chalopin, Y., Solonin, Y. M., and Volz, S. (2014), Tailoring properties of graphene with vacancies. *Phys. Status Solidi B*, **251**: 555–558. doi: 10.1002/pssb.201300301

[22] Zan R., Ramasse Q.M., Bangert U., and Novoselov K.S. Graphene (2012) Reknits Its Holes. *Nano Lett.* **12** (8), 3936–3940. doi: 10.1021/nl300985q

[23] L. Wang,F. Yan, H. L. W. Chanb, F. Ding, A structural stability diagram of multiple vacancies and defect self-healing in graphene, *Nanoscale*, 2012, **4**, 7489–7493.

[24] Botari T., Paupitz R., da Silva Autreto P.A., Galvao D. S. (2016) Graphene healing mechanisms: A theoretical investigation, *Carbon*, **99**, 302-309, doi:10.1016/j.carbon.2015.11.070.

[25] Özçelik, V.O., Gurel, H.H., Ciraci, S. (2013). Self-healing of vacancy defects in single-layer graphene and silicene. *Physical Review B*, **88**(4), 045440.

[26] Putz, M.V.; Ori, O.(2014) Bondonic Effects in Group-IV Honeycomb Nanoribbons with Stone-Wales Topological Defects. *Molecules*, **19**, 4157-4188. doi:10.3390/molecules19044157